

# Modeling Structure with Undirected Neural Networks

Tsvetomila Mihaylova<sup>1,2</sup>, Vlad Niculae<sup>4</sup>, and André F. T. Martins<sup>1,2,3</sup>

<sup>1</sup>Instituto de Telecomunicações, Lisbon, Portugal

<sup>2</sup>Instituto Superior Tecnico & LUMIS (Lisbon ELLIS Unit), Lisbon, Portugal

<sup>3</sup>Unbabel, Lisbon, Portugal

<sup>4</sup>Language Technology Lab, Informatics Institute, University of Amsterdam, The Netherlands

\*tsvetomila.mihaylova@lx.it.pt, v.niculae@uva.nl, andre.t.martins@tecnico.ulisboa.pt

## Abstract

Neural networks are powerful function estimators, leading to their status as a paradigm of choice for modeling structured data. However, unlike other structured representations that emphasize the modularity of the problem – *e.g.*, factor graphs – neural networks are usually monolithic mappings from inputs to outputs, with a fixed computation order. This limitation prevents them from capturing different directions of computation and interaction between the modeled variables.

In this paper, we combine the representational strengths of factor graphs and of neural networks, proposing *undirected neural networks (UNNs)*: a flexible framework for specifying computations that can be performed in any order. For particular choices, our proposed models subsume and extend many existing architectures: feed-forward, recurrent, self-attention networks, auto-encoders, and networks with implicit layers. We demonstrate the effectiveness of undirected neural architectures, both unstructured and structured, on a range of tasks: tree-constrained dependency parsing, convolutional image classification, and sequence completion with attention. By varying the computation order, we show how a single UNN can be used both as a classifier and a prototype generator, and how it can fill in missing parts of an input sequence, making them a promising field for further research.

Factor graphs have historically been a very appealing toolbox for representing structured prediction problems (Bakır et al., 2007; Smith, 2011; Nowozin et al., 2014), with wide applications to vision and natural language processing applications. In the last years, neural networks have taken over as the model of choice for tackling these applications. Unlike factor graphs – which emphasize the modularity of the problem –

neural networks typically work end-to-end, relying on rich representations captured at the encoder level (often pre-trained), which are then propagated to a task-specific decoder.

In this paper, we combine the representational strengths of factor graphs and neural networks by proposing **undirected neural networks (UNNs)** – a framework in which outputs are not computed by evaluating a composition of functions in a given order, but are rather obtained *implicitly* by minimizing an energy function which factors over a graph. For particular choices of factor potentials, UNNs subsume many existing architectures, including feedforward, recurrent, and self-attention neural networks, auto-encoders, and networks with implicit layers. When coupled with a coordinate-descent algorithm to minimize the energy, the computation performed in an UNN is similar (but not equivalent) to a neural network sharing parameters across multiple identical layers. Since UNNs have no prescribed computation order, the exact same network can be used to predict any group of variables (outputs) given another group of variables (inputs), or vice-versa (*i.e.*, inputs from outputs). Our contributions are:

- We present UNNs and show how they extend many existing neural architectures.
- We provide a coordinate descent inference algorithm, which, by an “unrolling lemma” (Lemma 1), can reuse current building blocks from feed-forward networks in a modular way.
- We develop and experiment with multiple factor graph architectures, tackling both structured and unstructured tasks, such as natural language parsing, image classification, and image prototype generation. We develop a new undirected attention mechanism and demonstrate its suitability for sequence completion.

**Notation.** We denote vector values as  $a$ , matrix and tensor values as  $A$ , and abstract factor graph variables as  $A$ . The Frobenius inner product of two tensors with matching dimensions

$A, B \in \mathbb{R}^{d_1 \times \dots \times d_n}$  is  $\langle A, B \rangle := \sum_{i_1=1}^{d_1} \dots \sum_{i_n=1}^{d_n} a_{i_1 \dots i_n} b_{i_1 \dots i_n}$ . For vectors  $\langle a, b \rangle = a^\top b$  and for matrices  $\langle A, B \rangle = \text{Tr}(A^\top B)$ . The Frobenius norm is  $\|A\| := \sqrt{\langle A, A \rangle}$ . Given two tensors  $A \in \mathbb{R}^{c_1, \dots, c_m}, B \in \mathbb{R}^{d_1, \dots, d_n}$ , their outer product is  $(A \otimes B)_{i_1, \dots, i_m, j_1, \dots, j_n} = a_{i_1, \dots, i_m} b_{j_1, \dots, j_n}$ . For vectors,  $a \otimes b = ab^\top$ . We denote the  $d$ -dimensional vector of ones as  $1_d$  (or tensor, if  $d$  is a tuple.) The Fenchel conjugate of a function  $\Psi: \mathbb{R}^d \rightarrow \mathbb{R}$  is  $\Psi^*(t) := \sup_{x \in \mathbb{R}^d} \langle x, t \rangle - \Psi(x)$ . When  $\Psi$  is strictly convex,  $\Psi^*$  is differentiable, and  $(\nabla \Psi^*)(t)$  is the unique maximizer  $\text{argmax}_{x \in \mathbb{R}^d} \langle x, t \rangle - \Psi(x)$ . We denote the non-negative reals as  $\mathbb{R}_+^d := \{x \in \mathbb{R}^d : x \geq 0\}$ , and the  $(d-1)$ -dimensional simplex as  $\Delta_d := \{\alpha \in \mathbb{R}_+^d, \langle 1_d, \alpha \rangle = 1\}$ . The Shannon entropy of a discrete distribution  $y \in \Delta_d$  is  $\mathcal{H}(y) := -\sum_i y_i \log y_i$ . The indicator function  $\iota_{\mathcal{X}}$  is defined as  $\iota_{\mathcal{X}}(x) := 0$  if  $x \in \mathcal{X}$ , and  $\iota_{\mathcal{X}}(x) := +\infty$  otherwise.

## 1. Undirected Neural Networks

Let  $\mathcal{G} = (V, F)$  be a factor graph, *i.e.*, a bipartite graph consisting of a set of variable nodes  $V$  and a set of factor nodes  $F$ , where each factor node  $f \in F \subseteq 2^V$  is linked to a subset of variable nodes. Each variable node  $X \in V$  is associated with a representation vector  $x \in \mathbb{R}^{d_X}$ . We define unary energies for each variable  $E_X(x)$ , as well as higher-order energies  $E_f(x_f)$ , where  $x_f$  denotes the values of all variables linked to factor  $f$ . Then, an assignment defines a total energy function

$$E(x_1, \dots, x_n) := \sum_i E_{X_i}(x_i) + \sum_f E_f(x_f). \quad (1)$$

For simple factor graphs where there is no ambiguity, we may refer to factors directly by the variables they link to. For instance, a simple fully-connected factor graph with only two variables  $X$  and  $Y$  is fully specified by  $E(x, y) = E_X(x) + E_Y(y) + E_{XY}(x, y)$ .

The energy function in Eq. (1) induces preferences for certain configurations. For instance, a globally best configuration can be found by solving  $\text{argmin}_{x, y} E(x, y)$ , while a best assignment for  $Y$  given a fixed value of  $X$  can be found by solving  $\text{argmin}_y E(x, y)$ .<sup>1</sup> We may think of, or suggest using notation, that  $X$  is an *input* and  $Y$  is an *output*. However, intrinsically, factor graphs are not attached to a static notion of input and output, and instead can be used to infer any subset of variables given any other subset.

In our proposed framework of UNNs, we define the computation performed by a neural network using a factor graph, where each variable is a representation vector (*e.g.*, analogous to the output of a layer in a standard network.) We design the factor energy functions depending on the type of each variable and the desired relationships between them. Inference is performed by minimizing the joint energy with respect to all unobserved

<sup>1</sup>In this work, we only consider deterministic inference in factor graphs. Probabilistic models are a promising extension.

variables (*i.e.*, hidden and output values). For instance, to construct a supervised UNN, we may designate a particular variable as “input”  $X$  and another as “output”  $Y$ , alongside several hidden variables  $H_i$ , compute

$$\hat{y} = \text{argmin}_y \min_{h_1, \dots, h_n} E(x, h_1, \dots, h_n, y), \quad (2)$$

and train by minimizing some loss  $\ell(\hat{y}, y)$ . However, UNNs are not restricted to the supervised setting or to a single input and output, as we shall explore.

While this framework is very flexible, Eq. (2) is a non-trivial optimization problem. Therefore, we focus on a class of energy functions that renders inference easier:

$$\begin{aligned} E_{X_i}(x_i) &= -\langle b_{X_i}, x_i \rangle + \Psi_{X_i}(x_i), \\ E_f(x_f) &= -\left\langle W_f, \bigotimes_{X_j \in f} x_j \right\rangle, \end{aligned} \quad (3)$$

where each  $\Psi_{X_i}$  is a strictly convex regularizer,  $\otimes$  denotes the outer product, and  $W_f$  is a parameter tensor of matching dimension. For pairwise factors  $f = \{X, Y\}$ , the factor energy is bilinear and can be written simply as  $E_{XY}(x, y) = -x^\top W y$ . In factor graphs of the form given in Eq. (3), the energy is convex in each variable separately, and block-wise minimization has a closed-form expression involving the Fenchel conjugate of the regularizers. This suggests a block coordinate descent optimization strategy: given an order  $\pi$ , iteratively set:

$$x_{\pi_j} \leftarrow \text{argmin}_{x_{\pi_j}} E(x_1, \dots, x_n). \quad (4)$$

This block coordinate descent algorithm is guaranteed to decrease energy and, for energies as in Eq. (3), converge to a Nash equilibrium (Xu & Yin, 2013, Thm. 2.3); in addition, it is conveniently learning-rate free. For training, to tackle the bi-level optimization problem, we unroll the coordinate descent iterations, and minimize some loss with standard deep learning optimizers, like stochastic gradient or Adam.

The following result, proved in Appendix A, shows that the coordinate descent algorithm (Eq. (4)) for UNNs with multilinear factor energies (Eq. (3)), corresponds to standard forward propagation on an unrolled neural network.

**Lemma 1** (Unrolling Lemma). *Let  $\mathcal{G} = (V, F)$  be a pairwise factor graph, with multilinear higher-order energies and strictly convex unary energies, as in Eq. (3). Then, the coordinate descent updates equation 4 result in a chain of affine transformations (*i.e.*, pre-activations) followed by non-linear activations, applied in the order  $\pi$ , yielding a traditional computation graph.*

The following examples demonstrate the lemma, and the flexibility of our framework.

Table 1: Examples of regularizers  $\Psi(h)$  corresponding to some common activation functions, where  $\phi(t) = t \log t$ .

$\Psi(h)$	$(\nabla \Psi^*)(t)$
$\frac{1}{2} \ h\ ^2$	$t$
$\frac{1}{2} \ h\ ^2 + \iota_{\mathbb{R}_+}(h)$	$\text{relu}(t)$
$\sum_j (\phi(h_j) + \phi(1-h_j)) + \iota_{[0,1]^d}(h)$	$\text{sigmoid}(t)$
$\sum_j (\phi(\frac{1+h_j}{2}) + \phi(\frac{1-h_j}{2})) + \iota_{[-1,1]^d}(h)$	$\tanh(t)$
$-\mathcal{H}(h) + \iota_{\Delta}(h)$	$\text{softmax}(t)$

**Single pairwise factor** The simplest possible UNN has a pairwise factor connecting two variables  $X, H$ . We may interpret  $X$  as an input, and  $H$  either as an output (in supervised learning) or a hidden representation in unsupervised learning (Fig. 2(a)). Bilinear-convex energies as in Eq. (3) yield:

$$\begin{aligned} E_{XH}(x, h) &= -\langle h, Wx \rangle, \\ E_X(x) &= -\langle x, b_X \rangle + \Psi_X(x), \\ E_H(h) &= -\langle h, b_H \rangle + \Psi_H(h). \end{aligned} \quad (5)$$

This resembles a Boltzmann machine with continuous variables (Smolensky, 1986; Hinton, 2007; Welling et al., 2004); however, in contrast to Boltzmann machines, we do not model joint probability distributions, but instead use factor graphs as representations of deterministic computation, more akin to computation graphs.

Given  $x$ , the updated  $h$  minimizing the energy is:

$$\begin{aligned} h_* &= \underset{h \in \mathbb{R}^M}{\text{argmin}} -(Wx + b_H)^\top h + \Psi_H(h) \\ &= (\nabla \Psi_H^*)(Wx + b_H), \end{aligned} \quad (6)$$

where  $\nabla \Psi_H^*$  is the gradient of the conjugate function of  $\Psi_H$ . Analogously, the update for  $X$  given  $H$  is:

$$x_* = (\nabla \Psi_X^*)(W^\top h + b_X). \quad (7)$$

Other than the connection to Boltzmann machines, one round of updates of  $H$  and  $X$  in this order also describe the computation of an auto-encoder with shared encoder/decoder weights.

Table 1 shows examples of regularizers  $\Psi$  and their corresponding  $\nabla \Psi^*$ . In practice, we never evaluate  $\Psi$  or  $\Psi^*$ , but only  $\nabla \Psi^*$ , which we choose among commonly-used neural network activation functions like  $\tanh$ ,  $\text{relu}$ , and  $\text{softmax}$ .

**Feed-forward neural networks** Any directed computation graph associated with a neural network is a particular case of an UNN. We illustrate this for a simple feed-forward network, which chains the functions  $h = f(x)$  and  $y = g(h)$ , where  $x \in \mathbb{R}^m$ ,  $h \in \mathbb{R}^d$ ,  $y \in \mathbb{R}^n$  are input, hidden, and output variables,

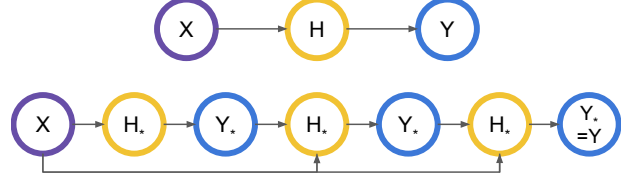


Figure 1: Unrolling the computation graph for undirected MLP with a single hidden layer. Top: MLP with one hidden layer. Bottom: Unrolled graph for UNN with  $k=3$  iterations.

and  $f: \mathbb{R}^m \rightarrow \mathbb{R}^d$  and  $g: \mathbb{R}^d \rightarrow \mathbb{R}^n$  are the functions associated to each layer (e.g., an affine transformation followed by a non-linearity). This factor graph is illustrated in Fig. 2(b). To see this, let  $V = \{X, H, Y\}$  and  $F = \{XH, HY\}$  and define the energies as follows. Let  $d: \mathbb{R}^d \times \mathbb{R}^d \rightarrow \mathbb{R}_+$  be any distance function satisfying  $d(a, b) \geq 0$ , with equality iff  $a = b$ ; for example  $d(a, b) = \|a - b\|$ . Let all the unary energies be zero and define the factor energies  $E_{XH}(x, h) = d(h, f(x))$  and  $E_{HY}(h, y) = d(y, g(h))$ . Then the total energy satisfies  $E(x, h, y) \geq 0$ , with equality iff the equations  $h = f(x)$  and  $y = g(h)$  are satisfied – therefore, the energy is minimized (and becomes zero) when  $y = g(f(x))$ , matching the corresponding directed computation graph. This can be generalized for an arbitrary deterministic neural network. This way, we can form UNNs that are partly directed, partly undirected, as the whole is still an UNN. We do this in our experiments in Section 4, where we fine-tune a pretrained BERT model appended to a UNN for parsing.

**Implicit layers** UNNs include networks with implicit layers (Duvenaud et al., 2020), a paradigm which, in contrast with feed-forward layers, does not specify how to compute the output from the input, but rather specifies conditions that the output layer should specify, often related to minimizing some function, e.g., computing a layer  $h_{i+1}$  given a previous layer  $h_i$  involves solving a possibly difficult problem  $\text{argmin}_h f(h_i, h)$ . Such a function  $f$  can be directly interpreted as an energy in our model, i.e.,  $E_{H_i H_{i+1}} = f$ .

**Undirected multi-layer perceptron (MLP)** Fig. 2(b) shows the factor graph for an undirected MLP analogous to a feed-forward one with input  $X$ , output  $Y$ , and a single hidden layer  $H$ . As in Eq. (3), we have bilinear pairwise factors

$$E_{XH}(x, h) = -\langle h, Wx \rangle, \quad E_{HY}(h, y) = -\langle y, Vh \rangle, \quad (8)$$

and linear-plus-convex unaries  $E_Z(x) = -\langle x, b_Z \rangle + \Psi_Z(x)$  for  $Z \in \{X, H, Y\}$ . If  $x$  is observed (fixed), coordinate-wise inference updates take the form:

$$\begin{aligned} h_* &= (\nabla \Psi_H^*)(Wx + V^\top y + b_H), \\ y_* &= (\nabla \Psi_Y^*)(Vh + b_Y). \end{aligned} \quad (9)$$

Note that  $E_X$  does not change anything if  $X$  is always observed. The entire algorithm can be unrolled into a directed

computation graph, leading to a deep neural network with shared parameters (Fig. 1).

The regularizers  $\Psi_H$  and  $\Psi_Y$  may be selected based on what we want  $\nabla\Psi^*$  to look like, and the constraints or domains of the variables. For instance, if  $Y$  is a multiclass classification output, we may pick  $\Psi_Y$  such that  $\nabla\Psi_Y^*$  be the softmax function, and  $\Psi_H$  to induce a relu nonlinearity. Initializing  $y^{(0)} = 0$  and performing a single iteration of updating  $H$  followed by  $Y$  results in a standard MLP with a single hidden layer (see also Fig. 1). However, the UNN point of view lets us decrease energy further by performing multiple iterations, as well as use the same model to infer any variables given any other ones, *e.g.*, to predict  $x$  from  $y$  instead of  $y$  from  $x$ . We demonstrate this power in Sections 2 to 4.

## 2. Image Classification and Visualization

Unlike feed-forward networks, where the processing order is hard-coded from inputs  $X$  to outputs  $Y$ , UNNs support processing in any direction. We can thus use the same trained network both for classification as well as for generating prototypical examples for each class. We demonstrate this on the MNIST dataset of handwritten digits (Deng, 2012), showcasing convolutional UNN layers.

The architecture is shown in Fig. 2(c) and has the following variables: the image  $X$ , the class label  $Y$  and two hidden layer variables  $H_{\{1,2\}}$ . Unlike the previous examples, the two pairwise energies involving the image and the hidden layers are convolutional, *i.e.*, linear layers with internal structure:

$$\begin{aligned} E_{XH_1}(X, H_1) &= -\langle H_1, \mathcal{C}_1(X; W_1) \rangle, \\ E_{H_1H_2}(H_1, H_2) &= -\langle H_2, \mathcal{C}_2(H_1; W_2) \rangle, \end{aligned} \quad (10)$$

where  $\mathcal{C}_{1,2}$  are linear cross-correlation operators with stride two and filter weights  $W_1 \in \mathbb{R}^{32 \times 1 \times 6 \times 6}$  and  $W_2 \in \mathbb{R}^{64 \times 32 \times 4 \times 4}$ . The last layer is fully connected:

$$E_{H_2Y}(H_2, y) = -\langle V, y \otimes H_2 \rangle. \quad (11)$$

The unary energies for the hidden layers contain standard (convolutional) bias term along with the binary entropy term  $\Psi_{\tanh}(H)$  such that  $\nabla\Psi_{\tanh}^*(t) = \tanh(t)$  (see Table 1). Note that  $X$  is no longer a constant when generating  $X$  given  $Y$ , therefore it is important to specify the unary energy  $E_X$ . Since pixel values are bounded, we set  $E_X(x) = \Psi_{\tanh}(x)$ . Initializing  $H_1, H_2$ , and  $y$  with zeroes and updating them once blockwise in this order yields exactly a feed-forward convolutional neural network. As our network is undirected, we may propagate information in multiple passes, proceeding in the order  $H_1, H_2, Y, H_2$  iteratively. The update for  $H_1$  involves a convolution of  $X$  and a deconvolution of  $H_2$ ; we defer the other updates to Appendix D:

$$(H_1)_* = \tanh(\mathcal{C}_1(X; W_1) + \mathcal{C}_2^\top(H_2; W_2) + b_1 \otimes 1_{d_1}), \quad (12)$$

where  $b_1 \in \mathbb{R}^{32}$  are biases for each filter, and  $d_1 = 12 \times 12$  is the convolved image size. To generate digit prototype

Table 2: MNIST accuracy with convolutional UNN.

ITERATIONS	ACCURACY
$k=1, \gamma=0$ (BASELINE)	98.64
$k=1$	98.60
$k=2$	98.73
$k=3$	98.72
$k=5$	98.73

$X$  from a given class  $c \in \{1, \dots, 10\}$ , we may set  $y = e_c$ , initialize the other variables at zero (including  $X$ ), and solve  $\hat{X} = \operatorname{argmin}_X \min_{H_{1,2}} E(X, H_1, H_2, y)$  by coordinate descent in the reverse order  $H_2, H_1, X, H_1$  iteratively.

We train our model jointly for both tasks. For each labeled pair  $(X, y)$  from the training data, we first predict  $\hat{y}$  given  $X$ , then separately predict  $\hat{X}$  given  $y$ . The incurred loss is a weighted combination  $\ell(x, y) = \ell_f(y, \hat{y}) + \gamma \ell_b(X, \hat{X})$ , where  $\ell_f$  is a 10-class cross-entropy loss, and  $\ell_b$  is a binary cross-entropy loss averaged over all  $28 \times 28$  pixels of the image. We use  $\gamma = .1$  and an Adam learning rate of .0005.

The classification results are shown in Table 2. The model is able to achieve high classification accuracy, and multiple iterations lead to a slight improvement. This result suggests the reconstruction loss for  $X$  can also be seen as a regularizer, as the same model weights are used in both directions. The more interesting impact of multiple energy updates is the image prototype generation. In Fig. 3 we show the generated digit prototypes after several iterations of energy minimization, as well as for models with a single iteration. The networks trained as UNNs produce recognizable digits, and in particular the model with more iterations learns to use the additional computation to produce clearer pictures. As for the baseline, we may interpret it as an UNN and apply the same process to extract prototypes, but this does not result in meaningful digits (Fig. 3c).

## 3. Undirected Attention Mechanism

Attention (Bahdanau et al., 2014; Vaswani et al., 2017) is a key component that enables neural networks to handle variable-length sequences as input. In this section, we propose an undirected attention mechanism (Fig. 2(e)). We demonstrate this model on the task of completing missing values in a sequence of dynamic length  $n$ , with the variable  $X$  serving as both input and output, taking values  $X \in \mathbb{R}^{d \times n}$ , queries, keys and values taking values  $Q, K, V \in \mathbb{R}^{n \times d}$ , and attention weights  $S \in (\Delta_n)^n$ , where  $d$  is a fixed hidden layer size. Finally,  $H$  is an induced latent sequence representation, with values  $H \in \mathbb{R}^{n \times d}$ . The only trainable parameters are  $W_Q, W_K, W_V \in \mathbb{R}^{d \times d}$ , and the input embeddings. We model scaled dot-product attention given with  $\operatorname{softmax}(d^{-\frac{1}{2}} Q K^\top) V$ . For all variables except  $S$ , we set  $E(\cdot) = \frac{1}{2} \|\cdot\|^2$ . For the attention weights, we use

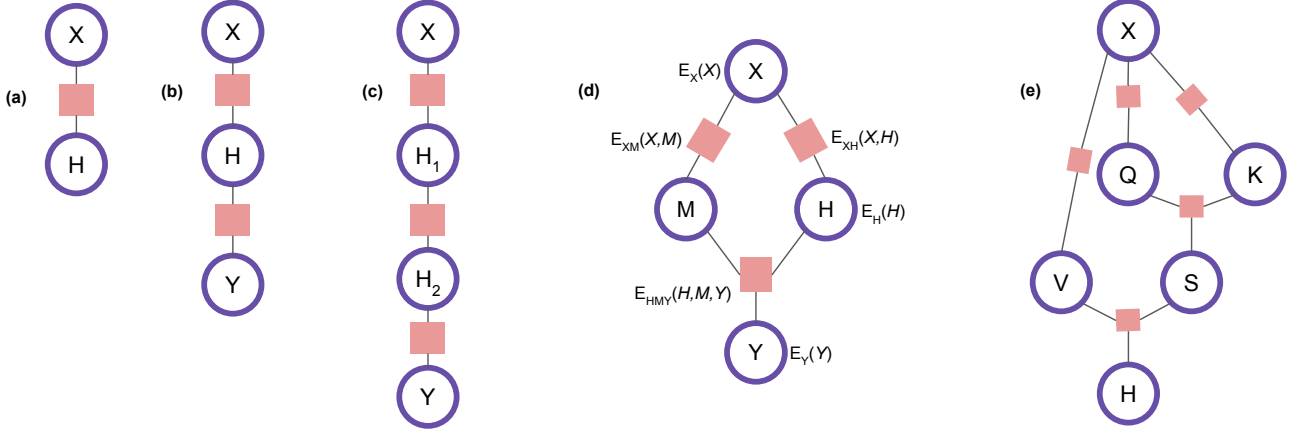


Figure 2: Factor graphs for: (a) network without intermediate layers, (b-c) undirected MLPs with one or two layers, (d) undirected biaffine dependency parser, (e) undirected self-attention. Energy labels omitted for brevity with the exception of (d).

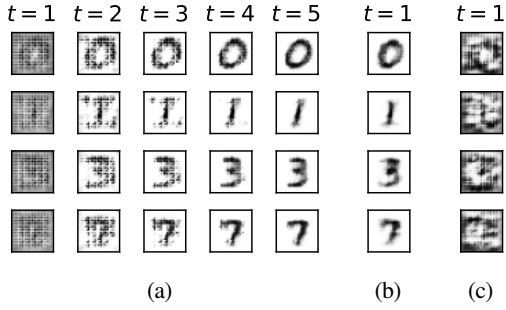


Figure 3: Digit prototypes generated by convolutional UNN. (a) best UNN ( $k=5, \gamma=.1$ ), (b) single iteration UNN ( $k=1, \gamma=.1$ ), (c): standard convnet ( $k=1, \gamma=0$ ). More in Appendix C.

$E_S(S) = -\sqrt{d} \sum_{i=1}^n \mathcal{H}(S_i)$ . The higher-order energies are:

$$\begin{aligned}
 E_{XQ}(X, Q) &= -\langle Q, W_Q(X+P) \rangle, \\
 E_{XK}(X, K) &= -\langle K, W_K(X+P) \rangle, \\
 E_{XV}(X, V) &= -\langle V, W_V(X+P) \rangle, \\
 E_{QKS}(Q, K, S) &= -\langle S, QK^\top \rangle, \\
 E_{VSH}(V, S, H) &= -\langle H, SV \rangle,
 \end{aligned} \tag{13}$$

where  $P$  is a matrix of sine and cosine positional embeddings of same dimensions as  $X$  (Vaswani et al., 2017).

Minimizing the energy yields the blockwise updates:

$$\begin{aligned}
 Q_\star &= W_Z(X+P) + SK, \\
 K_\star &= W_K(X+P) + S^\top Q, \\
 V_\star &= W_V(X+P) + S^\top H, \\
 S_\star &= \text{softmax}\left(d^{-1/2}(QK^\top + VH^\top)\right), \\
 H_\star &= SV, \\
 \bar{X}_\star &= \bar{V}W_V + \bar{Q}W_Q + \bar{K}W_K,
 \end{aligned} \tag{14}$$

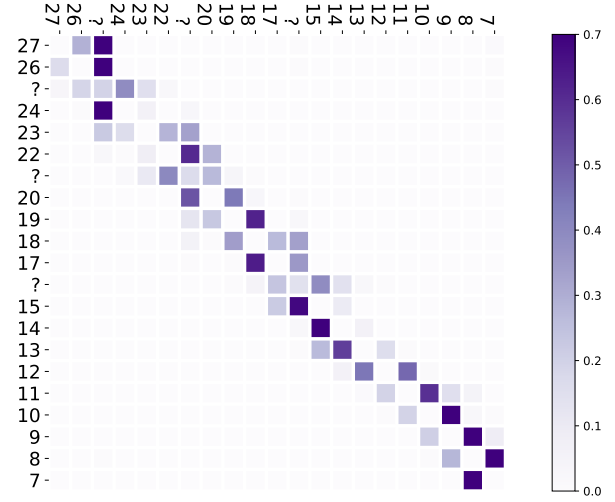


Figure 4: Undirected self-attention (one “forward-backward” pass) identifies an off-diagonal pattern, allowing generalization.

where  $\bar{X}$  denotes only the rows of  $X$  corresponding to the masked (missing) entries.

Provided zero initialization, updating in the order (V/Q/K), S, H corresponds exactly to a forward pass in a standard self-attention. However, in an UNN, our expressions allow backward propagation back toward  $X$ , as well as iterating to an equilibrium. To ensure that one round of updates propagates information through all the variables, we employ the “forward-backward” order  $Q, K, V, S, H, S, V, K, Q, \bar{X}$ .

We evaluate the performance of the undirected attention with a toy task of sequence completion. We generate a toy dataset of numerical sequences between 1 and 64, of length at least 8 and at most 25, in either ascending or descending consecutive order. We mask out up to 10% of the tokens and generate all possible sequences, splitting them into training and test sets with around

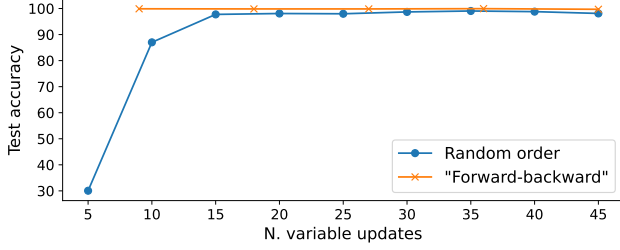


Figure 5: Comparison of the test accuracy for models with random and “forward-backward” order of variable updates. Markers indicate one full iteration.

706K and 78K instances. Undirected self-attention is applied to the input sequence. Note that because of the flexibility of the architecture, the update of the input variable  $X$  does not differ from the updates of the remaining variables, because each variable update corresponds to one step of coordinate descent. The model incurs a cross-entropy loss for the missing elements of the sequence and the parameters are updated using Adam with learning rate  $10^{-4}$ . The hidden dimension is  $d=256$ , and gradients with magnitude beyond 10 are clipped.

Undirected attention is able to solve this task, reaching over 99.8% test accuracy, confirming viability. Figure 4 shows the attention weights for a model trained with  $k=1$ . More attention plots are shown in Appendix C.

**Impact of update order.** The “forward-backward” order is not the only possible order of updates in an UNN. In Fig. 5 we compare its performance against a randomized coordinate descent strategy, where at each round we pick a permutation of  $Q, K, V, S, H$ . In both cases,  $X$  is updated at the end of each iteration. (Note that the “forward-backward” order performs almost twice the number of updates per iteration.) While the “forward-backward” order performs well even with a single pass, given sufficient iterations, random order updates can reach the same performance, suggesting that hand-crafting a meaningful order helps but is not necessary. Further analysis is reported in Appendix B.

#### 4. Structured UNNs for Dependency Parsing

The concept of UNN can be applied to structured tasks – all we need to do is to define *structured factors*, as shown next.

We experiment with a challenging structured prediction task from natural language processing: unlabeled, non-projective dependency parsing (Kübler et al., 2009). Given a sentence with  $n$  words, represented as a matrix  $X \in \mathbb{R}^{r \times n}$  (where  $r$  is the embedding size), the goal is to predict the syntactic relations as a *dependency tree*, i.e., a spanning tree which has the words as nodes. The output can be represented as a binary matrix  $Y \in \mathbb{R}^{n \times n}$ , where the  $(i, j)^{\text{th}}$  entry indicates if there is a directed arc  $i \rightarrow j$  connecting the  $i^{\text{th}}$  word (the *head*) and  $j^{\text{th}}$  word (the

*modifier*). Fig. 6 shows examples of dependency trees produced by this model. We use a probabilistic model where the output  $Y$  can more broadly represent a probability distribution over trees, represented by the matrix of arc marginals induced by this distribution (illustrated in Appendix C.)

**Biaffine parsing.** A successful model for dependency parsing is the biaffine one (Dozat & Manning, 2016; Kipewasser & Goldberg, 2016). This model first computes head representations  $H \in \mathbb{R}^{d \times n}$  and modifier representations  $M \in \mathbb{R}^{d \times n}$ , via a neural network that takes  $X$  as input – here,  $d$  denotes the hidden dimension of these representations. Then, it computes a score matrix as  $Z = H^\top V M \in \mathbb{R}^{n \times n}$ , where  $V \in \mathbb{R}^{d \times d}$  is a parameter matrix. Entries of  $Z$  can be interpreted as scores for each candidate arc. From  $Z$ , the most likely tree can be obtained via the Chu-Liu-Edmonds maximum spanning arborescence algorithm (Chu & Liu, 1965; Edmonds, 1967), and probabilities and marginals can be computed via the matrix-tree theorem (Koo et al., 2007; Smith & Smith, 2007; McDonald & Satta, 2007; Kirchhoff, 1847).

**UNN for parsing.** We now construct an UNN with the same building blocks as this biaffine model, leading to the factor graph in Fig. 2(d). The variable nodes are  $\{X, H, M, Y\}$ , and the factors are  $\{X_H, X_M, H_{YM}\}$ . Given parameter weight matrices  $V, W_H, W_M \in \mathbb{R}^{d \times d}$  and biases  $b_H, b_M \in \mathbb{R}^d$ , we use bilinear and trilinear factor energies as follows:

$$\begin{aligned} E_{X_H}(X, H) &= -\langle H, W_H X \rangle, \\ E_{X_M}(X, M) &= -\langle M, W_M X \rangle, \\ E_{Y_{HM}}(Y, H, M) &= -\langle Y, H^\top V M \rangle. \end{aligned} \quad (15)$$

For  $H$  and  $M$ , we use the ReLU regularizer,

$$\begin{aligned} E_H(H) &= -\langle b_H \otimes 1_n, H \rangle + \frac{1}{2} \|H\|^2 + \iota_{\geq 0}(H) \\ E_M(M) &= -\langle b_M \otimes 1_n, M \rangle + \frac{1}{2} \|M\|^2 + \iota_{\geq 0}(M). \end{aligned} \quad (16)$$

For  $Y$ , however, we employ a structured entropy regularizer:

$$E_Y(Y) = -\mathcal{H}_{\mathcal{M}}(Y) + \iota_{\mathcal{M}}(Y), \quad (17)$$

where  $\mathcal{M} = \text{conv}(\mathcal{Y})$  is the marginal polytope (Wainwright & Jordan, 2008; Martins et al., 2009), the convex hull of the adjacency matrices of all valid non-projective dependency trees (Fig. 10), and  $\mathcal{H}_{\mathcal{M}}(Y)$  is the maximal entropy over all distribution over trees with arc marginals  $Y$ :

$$\mathcal{H}_{\mathcal{M}}(Y) := \max_{\alpha \in \Delta_{|\mathcal{Y}|}} \mathcal{H}(\alpha) \text{ s.t. } \mathbb{E}_{A \sim \alpha}[A] = Y. \quad (18)$$

**Derivation of block coordinate descent updates.** To minimize the total energy, we iterate between updating  $H$ ,  $M$  and  $Y$   $k$  times, similar to the unstructured case.



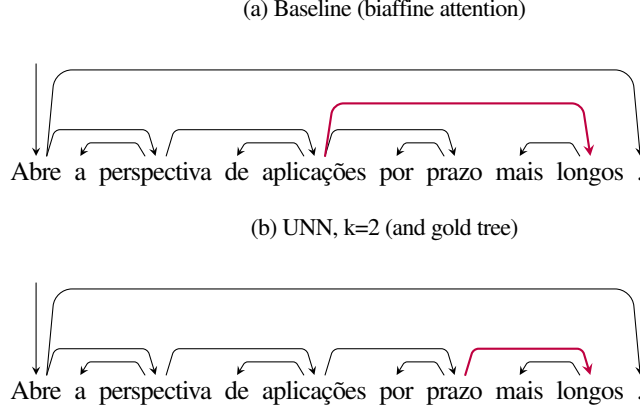


Figure 6: Examples of dependency trees produced by the parsing model for a sentence in Portuguese. The baseline model (a) erroneously assigns the noun *aplicações* as the syntactic head of the adjective *longos*. The UNN with  $k=2$  iterations (b) matches the gold parse tree for this sentence, eventually benefiting from the structural information propagated back from the node  $Y$  after the first iteration.

The updates for the heads and modifiers work out to:

$$\begin{aligned} H_{\star} &= \text{relu}(W_H X + b_H \otimes 1_n + V M Y^{\top}), \\ M_{\star} &= \text{relu}(W_M X + b_M \otimes 1_n + V^{\top} H Y). \end{aligned} \quad (19)$$

For  $Y$ , however, we must solve the problem

$$Y_{\star} = \underset{Y \in \mathcal{M}}{\text{argmin}} - \langle Y, H^{\top} V M \rangle - \mathcal{H}_{\mathcal{M}}(Y). \quad (20)$$

This combinatorial optimization problem corresponds to *marginal inference* (Wainwright & Jordan, 2008), a well-studied computational problem in structured prediction that appears in all probabilistic models. While generally intractable, for non-projective dependency parsing it may be computed in time  $\mathcal{O}(n^3)$  via the aforementioned matrix-tree theorem, the same algorithm required to compute the structured likelihood loss.<sup>2</sup>

With zero initialization, the first iteration yields the same hidden representations and output as the biaffine model, assuming the updates are performed in the order described. The extra terms involving  $V M Y^{\top}$  and  $V^{\top} H Y$  enable the current prediction for  $Y$  to influence neighboring words, which leads to a more expressive model overall.

**Experiments.** We experiment with the UNN for parsing described above. We test the architecture on several datasets from Universal Dependencies 2.7 (Zeman et al., 2020), covering different language families and dataset size: Afrikaans (AfriBooms), Arabic (PADT), Czech (PDT), English (Partut), Hungarian (Szeged), Italian (ISDT), Persian (Seraji), Portuguese (Bosque), Swedish (Talbanken), and Telugu (MTG). Performance is measured by three metrics:

- Unlabeled attachment score (UAS): a fine-grained, arc-level accuracy metric.
- Modifier list accuracy: the percentage of head words for which *all* modifiers were correctly predicted. For example, in Fig. 6, the baseline correctly predicts all modifiers for the words *perspectiva*, *abre*, *longos*, but not for the words *aplicações*, *prazo*.
- Exact match: the percentage sentences for which the full parse tree is correctly predicted: the harshest of the metrics.

The latter, coarser measures can give more information whether the model is able to learn global relations, not just how to make local predictions correctly (*i.e.*, when only prediction of the arcs is evaluated).

Our architecture is as follows: First, we pass the sentence through a BERT model (BERT-BASE-MULTILINGUAL-CASED, fine-tuned during training, as directed networks can be added as components to UNNs, as mentioned in Section 1) and get the word representations of the last layer. These representations are the input  $x$  in the UNN model. Then, we apply the parsing model described in this section. The baseline ( $k=1$ ) corresponds to a biaffine parser using BERT features. The learning rate for each language is chosen via grid search for highest UAS on the validation set for the baseline model. We searched over the values  $\{0.1, 0.5, 1, 5, 10\} \times 10^{-5}$ . In the experiments, we use  $10^{-5}$  for Italian and  $5 \times 10^{-5}$  for the other languages. We employ dropout regularization, using the same dropout mask for each variable throughout the inner coordinate descent iterations, so that dropped values do not leak.

The results from the parsing experiments are displayed in Table 3. The numbers in the table show results on the test set for the highest validation accuracy epoch. We see that some

<sup>2</sup>During training, the matrix-tree theorem can be invoked only once to compute both the update to  $Y$  as well as the gradient of the loss, since  $\nabla \log p(Y = Y_{\text{true}}) = Y_{\text{true}} - \hat{Y}$ .

Table 3: Results from experiments with parsing with structured UNNs. The columns show the number of UNN iterations. The best result for each row is rendered in bold.

LANGUAGE	$k=1$	$k=2$	$k=3$	$k=4$	$k=5$
UNLABELED ATTACHMENT SCORE					
AF	<b>89.09</b>	88.98	88.40	87.77	88.46
AR	<b>85.62</b>	84.94	84.22	83.69	83.63
CS	93.79	<b>93.83</b>	93.82	93.60	93.77
EN	91.96	91.86	91.09	<b>91.99</b>	91.51
FA	<b>83.41</b>	83.27	82.95	83.37	83.27
HU	85.11	<b>85.77</b>	84.47	85.13	84.09
IT	<b>94.76</b>	94.43	94.35	94.59	94.45
PT	96.99	97.00	96.83	<b>97.06</b>	96.90
SW	<b>91.42</b>	90.92	91.30	91.08	90.98
TE	89.72	89.72	<b>90.00</b>	88.45	87.75
MODIFIER LIST ACCURACY					
AF	<b>74.10</b>	72.60	72.90	71.78	72.01
AR	<b>70.44</b>	69.29	68.41	68.08	68.19
CS	84.46	84.82	<b>84.93</b>	84.12	84.49
EN	79.08	77.73	75.20	78.90	<b>79.44</b>
FA	64.80	<b>66.75</b>	65.28	66.67	65.85
HU	64.13	<b>66.07</b>	64.37	62.91	64.13
IT	<b>85.32</b>	83.59	83.71	83.94	84.05
PT	90.10	<b>90.69</b>	90.39	90.66	90.49
SW	<b>79.07</b>	78.37	78.52	78.60	78.24
TE	72.87	72.87	<b>73.68</b>	66.80	65.99
EXACT MATCH					
AF	<b>37.70</b>	33.88	34.43	33.88	32.79
AR	19.44	19.29	18.36	<b>19.91</b>	18.36
CS	59.17	60.76	<b>60.92</b>	59.42	59.84
EN	<b>48.59</b>	44.37	40.14	43.66	44.37
FA	21.52	22.15	22.78	<b>24.68</b>	23.42
HU	21.13	23.40	<b>24.15</b>	23.40	21.51
IT	<b>64.93</b>	63.54	62.85	63.89	64.24
PT	73.24	<b>74.86</b>	73.89	74.43	74.11
SW	<b>54.62</b>	52.38	54.13	53.94	52.67
TE	75.69	77.08	<b>79.17</b>	71.53	70.14

of the languages seem to benefit from the iterative procedure of UNNs (CS, HU, TE), while others do not (EN, AF), and little difference is observed in the remaining languages. In general, the baseline ( $k=1$ ) seems to attain higher accuracies in UAS (individual arcs), but most of the languages have overall more accurate structures (as measured by modifier list accuracy and by exact match) for  $k>1$ . Fig. 6 illustrates with one example in Portuguese.

## 5. Related Work

Besides the models mentioned in Section 1 which may be regarded as particular cases of UNNs, other models and architectures, next described, bear relation to our work.

**Probabilistic modeling of joint distributions** Our work draws inspiration from the well-known Boltzmann machines and Hopfield networks (Ackley et al., 1985; Smolensky, 1986; Hopfield, 1984). We consider deterministic networks whose desired configurations minimize an energy function which decomposes as a factor graph. In contrast, many other works have studied probabilistic energy-based models (EBM) defined as Gibbs distributions, as well as efficient methods to learn those distributions and to sample from them (Ngiam et al., 2011; Du & Mordatch, 2019). Similar to how our convolutional UNN can be used for multiple purposes in Section 2, Grathwohl et al. (2020a) reinterprets standard discriminative classifiers  $p(y|x)$  as an EBM of a joint distribution  $p(x,y)$ . Training stochastic EBMs requires Monte Carlo sampling or auxiliary networks (Grathwohl et al., 2020b); in contrast, our deterministic UNNs, more aligned conceptually with deterministic EBMs (LeCun et al., 2006), eschew probabilistic modeling in favor of more direct training. Moreover, our UNN architectures closely parallel feed-forward networks and reuse their building blocks, uniquely bridging the two paradigms.

**Structured Prediction Energy Networks (SPENs)** We saw in Section 4 that UNNs can handle structured outputs. An alternative framework for expressive structured prediction is given by SPENs (Belanger & McCallum, 2016). Most SPEN inference strategies require gradient descent, often with higher-order gradients for learning (Belanger et al., 2017), or training separate inference networks (Tu et al., 2020). UNNs in contrast, are well suited for coordinate descent inference: a learning-rate free algorithm with updates based on existing neural network building blocks. An undirected variant of SPENs would be similar to the MLP factor graph in Fig. 2(b), but with X and Y connected to a joint, higher-order factor, rather than via a chain  $X-H-Y$ .

**Universal transformers and Hopfield networks** In Section 3 we show how we can implement self-attention with UNNs. Performing multiple energy updates resembles – but is different from – transformers (Vaswani et al., 2017) with shared weights between the layers. Our perspective of minimizing UNNs with coordinate descent using a fixed schedule and this unrolling is similar (but not exactly the same due to the skip connections) to having deeper neural networks which shared parameters for each layer. Such an architecture is the Universal Transformer (Dehghani et al., 2018), which applies a recurrent neural network to the transformer encoder and decoder. Recent work (Ramsauer et al., 2020) shows that the self-attention layers of transformers can be regarded as the update rule of a Hopfield network with continuous states (Hopfield, 1984). This leads to a “modern Hopfield network” with continuous states and an update rule which ensures global convergence to stationary points of the energy (local minima or saddle points). Like that model, UNNs also seek local minima of an energy function, albeit with a different goal.



## 6. Conclusions and Future Work

We presented UNNs – a structured energy-based model which combines the power of factor graphs and neural networks. At inference time, the model energy is minimized with a coordinate descent algorithm, allowing reuse of existing building blocks in a modular way with guarantees of decreasing the energy at each step. We showed how the proposed UNNs subsume many existing architectures, conveniently combining supervised and unsupervised/self-supervised learning, as demonstrated on the three tasks.

We hope our first steps in this work will spark multiple directions of future work on undirected networks. One promising direction is on probabilistic UNNs with Gibbs sampling, which have the potential to bring our modular architectures to generative models. Another direction is to consider alternate training strategies for UNNs. Our strategy of converting UNNs to unrolled neural networks, enabled by Lemma 1, makes gradient-based training easy to implement, but alternate training strategies, perhaps based on equilibrium conditions or dual decomposition, hold promise.

## Acknowledgements

We would like to thank Mário Figueiredo, Caio Corro and the DeepSPIN team for helpful discussions. TM and AM are supported by the European Research Council (ERC StG DeepSPIN 758969), the P2020 program MAIA (LISBOA-01-0247- FEDER-045909), and by the Fundação para a Ciência e Tecnologia through contract UIDB/50008/2020. VN is partially supported by the Hybrid Intelligence Centre, a 10-year programme funded by the Dutch Ministry of Education, Culture and Science through the Netherlands Organisation for Scientific Research (<https://hybrid-intelligence-centre.nl>).

## References

- David H Ackley, Geoffrey E Hinton, and Terrence J Sejnowski. A learning algorithm for boltzmann machines. *Cognitive science*, 9(1):147–169, 1985.
- Dzmitry Bahdanau, Kyunghyun Cho, and Yoshua Bengio. Neural machine translation by jointly learning to align and translate. *arXiv preprint arXiv:1409.0473*, 2014.
- Gökhan Bakır, Thomas Hofmann, Alexander J Smola, Bernhard Schölkopf, and Ben Taskar. *Predicting structured data*. MIT press, 2007.
- David Belanger and Andrew McCallum. Structured prediction energy networks. In *International Conference on Machine Learning*, pp. 983–992. PMLR, 2016.
- David Belanger, Bishan Yang, and Andrew McCallum. End-to-end learning for structured prediction energy networks. In *International Conference on Machine Learning*, pp. 429–439. PMLR, 2017.
- Yoeng-Jin Chu and Tseng-Hong Liu. On the shortest arborescence of a directed graph. *Science Sinica*, 14: 1396–1400, 1965.
- Mostafa Dehghani, Stephan Gouws, Oriol Vinyals, Jakob Uszkoreit, and Lukasz Kaiser. Universal transformers. In *International Conference on Learning Representations*, 2018.
- Li Deng. The mnist database of handwritten digit images for machine learning research. *IEEE Signal Processing Magazine*, 29(6):141–142, 2012.
- Timothy Dozat and Christopher D Manning. Deep biaffine attention for neural dependency parsing. *arXiv preprint arXiv:1611.01734*, 2016.
- Yi-lun Du and Igor Mordatch. Implicit generation and modeling with energy based models. In *NeurIPS*, 2019.
- David Duvenaud, J Zico Kolter, and Matthew Johnson. Deep implicit layers tutorial-neural odes, deep equilibrium models, and beyond. *Neural Information Processing Systems Tutorial*, 2020.
- Jack Edmonds. Optimum branchings. *J. Res. Nat. Bur. Stand.*, 71B:233–240, 1967.
- Will Grathwohl, Kuan-Chieh Wang, Joern-Henrik Jacobsen, David Duvenaud, Mohammad Norouzi, and Kevin Swersky. Your classifier is secretly an energy based model and you should treat it like one. In *International Conference on Learning Representations*, 2020a.
- Will Grathwohl, Kuan-Chieh Wang, Jörn-Henrik Jacobsen, David Duvenaud, and Richard Zemel. Learning the stein discrepancy for training and evaluating energy-based models without sampling. In *ICML*. PMLR, 2020b.
- Geoffrey E Hinton. Boltzmann machine. *Scholarpedia*, 2(5): 1668, 2007.
- John J Hopfield. Neurons with graded response have collective computational properties like those of two-state neurons. *Proceedings of the national academy of sciences*, 81(10): 3088–3092, 1984.
- Eliyahu Kiperwasser and Yoav Goldberg. Simple and accurate dependency parsing using bidirectional LSTM feature representations. *Transactions of the Association for Computational Linguistics*, 4: 313–327, 2016. doi: 10.1162/tacl\_a\_00101. URL <https://www.aclweb.org/anthology/Q16-1023>.
- Gustav Kirchhoff. Ueber die auflösung der gleichungen, auf welche man bei der untersuchung der linearen vertheilung galvanischer ströme geführt wird. *Annalen der Physik*, 148 (12):497–508, 1847.

- Terry Koo, Amir Globerson, Xavier Carreras Pérez, and Michael Collins. Structured prediction models via the matrix-tree theorem. In *Joint Conference on Empirical Methods in Natural Language Processing and Computational Natural Language Learning (EMNLP-CoNLL)*, pp. 141–150, 2007.
- Sandra Kübler, Ryan McDonald, and Joakim Nivre. Dependency parsing. *Synthesis lectures on human language technologies*, 1(1):1–127, 2009.
- Yann LeCun, Sumit Chopra, Raia Hadsell, M Ranzato, and F Huang. A tutorial on energy-based learning. *Predicting structured data*, 1(0), 2006.
- André FT Martins, Noah A Smith, and Eric P Xing. Polyhedral outer approximations with application to natural language parsing. In *Proceedings of the 26th Annual International Conference on Machine Learning*, pp. 713–720, 2009.
- Ryan McDonald and Giorgio Satta. On the complexity of non-projective data-driven dependency parsing. In *Proceedings of the Tenth International Conference on Parsing Technologies*, pp. 121–132, 2007.
- Jiquan Ngiam, Zhenghao Chen, Pang Wei Koh, and Andrew Y Ng. Learning deep energy models. In *ICML*, 2011.
- Sebastian Nowozin, Peter V Gehler, Jeremy Jancsary, and Christoph H Lampert. *Advanced Structured Prediction*. MIT Press, 2014.
- Hubert Ramsauer, Bernhard Schäfl, Johannes Lehner, Philipp Seidl, Michael Widrich, Lukas Gruber, Markus Holzleitner, Milena Pavlović, Geir Kjetil Sandve, Victor Greiff, et al. Hopfield networks is all you need. *arXiv preprint arXiv:2008.02217*, 2020.
- David A Smith and Noah A Smith. Probabilistic models of nonprojective dependency trees. In *Proceedings of the 2007 Joint Conference on Empirical Methods in Natural Language Processing and Computational Natural Language Learning (EMNLP-CoNLL)*, pp. 132–140, 2007.
- Noah A Smith. Linguistic structure prediction. *Synthesis lectures on human language technologies*, 4(2):1–274, 2011.
- Paul Smolensky. Information processing in dynamical systems: Foundations of harmony theory. Technical report, Colorado Univ at Boulder Dept of Computer Science, 1986.
- Lifu Tu, Richard Yuanzhe Pang, and Kevin Gimpel. Improving joint training of inference networks and structured prediction energy networks. In *Proceedings of the Fourth Workshop on Structured Prediction for NLP*, pp. 62–73, Online, November 2020. Association for Computational Linguistics. doi: 10.18653/v1/2020.spnlp-1.8. URL <https://aclanthology.org/2020.spnlp-1.8>.
- Ashish Vaswani, Noam Shazeer, Niki Parmar, Jakob Uszkoreit, Llion Jones, Aidan N Gomez, Łukasz Kaiser, and Illia Polosukhin. Attention is all you need. In *Advances in Neural Information Processing Systems*, 2017.
- Martin J Wainwright and Michael Irwin Jordan. *Graphical models, exponential families, and variational inference*. Now Publishers Inc, 2008.
- Max Welling, Michal Rosen-Zvi, and Geoffrey Hinton. Exponential family harmoniums with an application to information retrieval. In *Proceedings of the 17th International Conference on Neural Information Processing Systems*, 2004.
- Yangyang Xu and Wotao Yin. A block coordinate descent method for regularized multiconvex optimization with applications to nonnegative tensor factorization and completion. *SIAM Journal on Imaging Sciences*, 6(3):1758–1789, 2013.
- Daniel Zeman, Joakim Nivre, Mitchell Abrams, Elia Ackermann, Noëmi Aepli, Hamid Aghaei, Željko Agić, Amir Ahmadi, Lars Ahrenberg, Chika Kennedy Ajede, Gabrielë Aleksandravičiūtė, Ika Alfina, Lene Antonsen, Katya Aplonova, Angelina Aquino, Carolina Aragon, Maria Jesus Aranzabe, Hórunn Arnardóttir, Gashaw Arutie, Jessica Naraiswari Arwidarasti, Masayuki Asahara, Luma Ateyah, Furkan Atmaca, Mohammed Attia, Aitziber Atutxa, Liesbeth Augustinus, Elena Badmaeva, Keerthana Balasubramani, Miguel Ballesteros, Esha Banerjee, Sebastian Bank, Verginica Barbu Mititelu, Victoria Basmov, Colin Batchelor, John Bauer, Seyyit Talha Bedir, Kepa Bengoetxea, Gözde Berk, Yevgeni Berzak, Irshad Ahmad Bhat, Riyaz Ahmad Bhat, Erica Biagetti, Eckhard Bick, Agnė Bielinskienė, Kristín Bjarnadóttir, Rogier Blokland, Victoria Bobicev, Loïc Boizou, Emanuel Borges Völker, Carl Börstell, Cristina Bosco, Gosse Bouma, Sam Bowman, Adriane Boyd, Kristina Brokaitė, Aljoscha Burchardt, Marie Candito, Bernard Caron, Gauthier Caron, Tatiana Cavalcanti, Gülşen Cebiroğlu Eryiğit, Flavio Massimiliano Cecchini, Giuseppe G. A. Celano, Slavomír Čéplö, Savas Cetin, Özlem Çetinoğlu, Fabricio Chalub, Ethan Chi, Yongseok Cho, Jinho Choi, Jayeol Chun, Alessandra T. Cignarella, Silvie Cinková, Aurélie Collomb, Çağrı Çöltekin, Miriam Connor, Marine Courtin, Elizabeth Davidson, Marie-Catherine de Marneffe, Valeria de Paiva, Mehmet Oguz Derin, Elvis de Souza, Arantza Diaz de Ilarraza, Carly Dickerson, Arawinda Dinakaramani, Bamba Dione, Peter Dirix, Kaja Dobrovoljc, Timothy Dozat, Kira Droganova, Puneet Dwivedi, Hanne Eckhoff, Marhaba Eli, Ali Elkahky, Binyam Ephrem, Olga Erina, Tomaž Erjavec, Aline Etienne, Wograinne Evelyn, Sidney Facundes, Richárd Farkas, Marília Fernanda, Hector Fernandez Alcalde, Jennifer Foster, Cláudia Freitas, Kazunori Fujita, Katarína Gajdošová, Daniel Galbraith, Marcos Garcia, Moa Gärdenfors, Sebastian Garza, Fabrício Ferraz Gerardi, Kim Gerdes, Filip Ginter, Iakes Goenaga, Koldo Gojenola, Memduh Gökırmak, Yoav Goldberg, Xavier Gómez Guinovart,

Berta González Saavedra, Bernadeta Griciūtė, Matias Gri-  
oni, Loïc Grobol, Normunds Grūzītis, Bruno Guillaume,  
Céline Guillot-Barbance, Tunga Güngör, Nizar Habash, Hin-  
rik Hafsteinsson, Jan Hajič, Jan Hajič jr., Mika Hämäläinen,  
Linh Hà Mỹ, Na-Rae Han, Muhammad Yudistira Hanif-  
muti, Sam Hardwick, Kim Harris, Dag Haug, Johannes  
Heinecke, Oliver Hellwig, Felix Hennig, Barbora Hladká,  
Jaroslava Hlaváčová, Florinel Hociung, Petter Hohle, Eva  
Huber, Jena Hwang, Takumi Ikeda, Anton Karl Ingason,  
Radu Ion, Elena Irimia, Olájiḡé Ishola, Tomáš Jelínek,  
Anders Johannsen, Hildur Jónsdóttir, Fredrik Jørgensen,  
Markus Juutinen, Sarveswaran K, Hüner Kaşıkara, An-  
dre Kaasen, Nadezhda Kabaeva, Sylvain Kahane, Hiroshi  
Kanayama, Jenna Kanerva, Boris Katz, Tolga Kayade-  
len, Jessica Kenney, Václava Kettnerová, Jesse Kirchner,  
Elena Klementieva, Arne Köhn, Abdullatif Köksal, Kamil  
Kopacewicz, Timo Korkiakangas, Natalia Kotsyba, Jolanta  
Kovalevskaitė, Simon Krek, Parameswari Krishnamurthy,  
Sookyoung Kwak, Veronika Laippala, Lucia Lam, Lorenzo  
Lambertino, Tatiana Lando, Septina Dian Larasati, Alexei  
Lavrentiev, John Lee, Phuong Lê Hồng, Alessandro Lenci,  
Saran Lertpradit, Herman Leung, Maria Levina, Cheuk Ying  
Li, Josie Li, Keying Li, Yuan Li, KyungTae Lim, Kris-  
ter Lindén, Nikola Ljubešić, Olga Loginova, Andry Luthfi,  
Mikko Luukko, Olga Lyashevskaya, Teresa Lynn, Vivien  
Macketanz, Aibek Makazhanov, Michael Mandl, Christo-  
pher Manning, Ruli Manurung, Cătălina Măranduc, David  
Mareček, Katrin Marheinecke, Héctor Martínez Alonso,  
André Martins, Jan Mašek, Hiroshi Matsuda, Yuji Mat-  
sumoto, Ryan McDonald, Sarah McGuinness, Gustavo Men-  
donça, Niko Miekka, Karina Mischenkova, Margarita Misir-  
pashayeva, Anna Missilä, Cătălin Mititelu, Maria Mitro-  
fan, Yusuke Miyao, AmirHossein Mojiri Foroushani, Amir-  
saeid Moloodi, Simonetta Montemagni, Amir More, Laura  
Moreno Romero, Keiko Sophie Mori, Shinsuke Mori, To-  
mohiko Morioka, Shigeki Moro, Bjartur Mortensen, Bohdan  
Moskalevskyi, Kadri Muischnek, Robert Munro, Yugo Mu-  
rawaki, Kaili Müürisep, Pinkey Nainwani, Mariam Nakhlé,  
Juan Ignacio Navarro Horñiácek, Anna Nedoluzhko, Gunta  
Nešpore-Bērzkalne, Luong Nguyễn Thị, Huyền Nguyễn  
Thị Minh, Yoshihiro Nikaido, Vitaly Nikolaev, Rattima Ni-  
tisaroj, Alireza Nourian, Hanna Nurmi, Stina Ojala, Atul Kr.  
Ojha, Adédayo Olúòkun, Mai Omura, Emeka Onwuegbuzia,  
Petya Osenova, Robert Östling, Lilja Øvrelid, Şaziye Betül  
Özateş, Arzucan Özgür, Balkız Öztürk Başaran, Niko Par-  
tanen, Elena Pascual, Marco Passarotti, Agnieszka Pate-  
juk, Guilherme Paulino-Passos, Angelika Peljak-Łapińska,  
Siyao Peng, Cenel-Augusto Perez, Natalia Perkova, Guy  
Perrier, Slav Petrov, Daria Petrova, Jason Phelan, Jussi Pi-  
itulainen, Tommi A Pirinen, Emily Pitler, Barbara Plank,  
Thierry Poibeau, Larisa Ponomareva, Martin Popel, Lauma  
Pretkalniņa, Sophie Prévost, Prokopis Prokopidis, Adam  
Przepiórkowski, Tiina Puolakainen, Sampo Pyysalo, Peng  
Qi, Andriela Rääbis, Alexandre Rademaker, Taraka Rama,

Loganathan Ramasamy, Carlos Ramisch, Fam Rashel, Mo-  
hammad Sadegh Rasooli, Vinit Ravishankar, Livy Real,  
Petru Rebeja, Siva Reddy, Georg Rehm, Ivan Riabov,  
Michael Rießler, Erika Rimkutė, Larissa Rinaldi, Laura Ri-  
tuma, Luisa Rocha, Eiríkur Rögnvaldsson, Mykhailo Roma-  
nenko, Rudolf Rosa, Valentin Roşca, Davide Rovati, Olga  
Rudina, Jack Rueter, Kristján Rúnarsson, Shoval Sadde, Pe-  
gah Safari, Benoît Sagot, Aleks Sahala, Shadi Saleh, Alessio  
Salomoni, Tanja Samardžić, Stephanie Samson, Manuela  
Sanguinetti, Dage Särg, Baiba Saulīte, Yanin Sawanaku-  
nanon, Kevin Scannell, Salvatore Scarlata, Nathan Schnei-  
der, Sebastian Schuster, Djamé Seddah, Wolfgang Seeker,  
Mojgan Seraji, Mo Shen, Atsuko Shimada, Hiroyuki Shi-  
rasu, Muh Shohibussirri, Dmitry Sichinava, Einar Freyr Sig-  
urdsson, Aline Silveira, Natalia Silveira, Maria Simi, Radu  
Simionescu, Katalin Simkó, Mária Šimková, Kiril Simov,  
Maria Skachedubova, Aaron Smith, Isabela Soares-Bastos,  
Carolyn Spadine, Steinhór Steingrímsson, Antonio Stella,  
Milan Straka, Emmett Strickland, Jana Strnadová, Alane  
Suhr, Yogi Lesmana Sulestio, Umut Sulubacak, Shingo  
Suzuki, Zsolt Szántó, Dima Taji, Yuta Takahashi, Fabio  
Tamburini, Mary Ann C. Tan, Takaaki Tanaka, Samson  
Tella, Isabelle Tellier, Guillaume Thomas, Liisi Torga, Mar-  
sida Toska, Trond Trosterud, Anna Trukhina, Reut Tsarfaty,  
Utku Türk, Francis Tyers, Sumire Uematsu, Roman Un-  
tilov, Zdeňka Urešová, Larraitz Uria, Hans Uszkoreit, An-  
drius Utkā, Sowmya Vajjala, Daniel van Niekerk, Gertjan  
van Noord, Viktor Varga, Eric Villemonte de la Clergerie,  
Veronika Vincze, Aya Wakasa, Joel C. Wallenberg, Lars  
Wallin, Abigail Walsh, Jing Xian Wang, Jonathan North  
Washington, Maximilian Wendt, Paul Widmer, Seyi Williams,  
Mats Wirén, Christian Wittem, Tsegay Woldemariam, Tak-  
sum Wong, Alina Wróblewska, Mary Yako, Kayo Yamashita,  
Naoki Yamazaki, Chunxiao Yan, Koichi Yasuoka, Marat M.  
Yavrumyan, Zhuoran Yu, Zdeněk Žabokrtský, Shorouq  
Zahra, Amir Zeldes, Hanzhi Zhu, and Anna Zhuravleva. Uni-  
versal dependencies 2.7, 2020. URL <http://hdl.handle.net/11234/1-3424>. LINDAT/CLARIAH-CZ digital library  
at the Institute of Formal and Applied Linguistics (ÚFAL),  
Faculty of Mathematics and Physics, Charles University.

## A. Proof of Lemma 1

We provide a more general proof for multilinear factor potentials, of which bilinear potentials are a special case. Let  $\mathcal{G} = (V, F)$  be the factor graph underlying the UNN, with energy function  $E(x_1, \dots, x_n) = \sum_i E_{X_i}(x_i) + \sum_f E_f(x_f)$ . We assume  $E_{X_i}(x_i) = -b_i^\top x_i + \Psi_{X_i}(x_i)$  for each  $X_i \in V$ , with  $\Psi_{X_i}$  convex, and  $E_f(x_f) = -\langle W_f, \bigotimes_{j \in f} x_j \rangle$  for each higher order factor  $f \in F$  (multilinear factor energy), where  $\bigotimes$  is the outer product, and  $W_f$  is a parameter tensor of matching dimension. For pairwise factors  $f = \{X_i, X_j\}$ , the factor energy is bilinear and can be written simply as  $E_f(x_i, x_j) = -x_i^\top W_f x_j$ .

The (block) coordinate descent algorithm updates each representation  $x_i \in V$  sequentially, leaving the remaining representations fixed. Let  $F(X_i) = \{f \in F : X_i \in f\} \subseteq F$  denote the set of factors  $X_i$  is linked to. The updates can be written as:

$$\begin{aligned} (x_i)_* &= \underset{x_i}{\operatorname{argmin}} E_{X_i}(x_i) + \sum_{f \in F(X_i)} E_f(x_f) \\ &= \underset{x_i}{\operatorname{argmin}} \Psi_{X_i}(x_i) - b_i^\top x_i - \underbrace{\sum_{f \in F(X_i)} \langle W_f, \bigotimes_{j \in f} x_j \rangle}_{-z_i^\top x_i} \\ &= (\nabla \Psi_{X_i}^*)(z_i), \end{aligned} \tag{21}$$

where  $z_i$  is a pre-activation given by

$$z_i = \left( \sum_{f \in F(X_i)} \rho_i(W_f) \bigotimes_{j \in f, j \neq i} x_j \right) + b_i, \tag{22}$$

and  $\rho_i$  is the linear operator that reshapes and rolls the axis of  $W_f$  corresponding to  $x_i$  to the first position. If all factors are pairwise, the update is more simply:

$$(x_i)_* = (\nabla \Psi_{X_i}^*) \left( \sum_{f = \{X_i, X_j\} \in F(X_i)} \rho_i(W_f) x_j + b_i \right), \tag{23}$$

where  $\rho_i$  is either the identity or the transpose operator. The update thus always consists in applying a (generally non-linear) transformation  $\nabla \Psi_{X_i}^*$  to an affine transformation of the neighbors of  $X_i$  in the graph (that is, the variables that co-participate in some factor).

Therefore, given any topological order of the variable nodes in  $V$ , running  $k$  iterations of the coordinate descent algorithm following that topological order is equivalent to performing forward propagation in an (unrolled) directed acyclic graph, where each node applies affine transformations on input variables followed by the activation function  $\nabla \Psi_{X_i}^*$ .

## B. Analysis of Order and Number of Variable Updates

For one of the experiments - undirected self-attention, we analyze how the order of variable updates and the number of update passes during training affect the model performance.

**Order of variable updates.** In Section 3 we showed that one pass of the “forward-backward” order or variable updates (Q,K,V,S,H,S,V,K,Q, $\hat{X}$ ) performs well enough for the of sequence completion. Since the flexibility of our model does not limit us to a specific order, we compare it to a random order of updating the variables (a permutation of Q,K,V,S,H;  $\hat{X}$  is always updated last). One pass over the “forward-backward” order performs nine variable updates, and one pass over the random order - five. In Fig. 5 we show how the two ways of order perform for different number of variable updates (for example, 2 passes over the “forward-backward” model equal 18 variable updates, and over the random model - 10). The “forward-backward” order performs best, but the random order can achieve similar performance after enough number of updates.

**Number of Energy Update Iterations** In addition to comparing the number of energy update iterations  $k$ , we also try setting a random number of updates during training. Instead of specifying a fixed number of iterations  $k$ , we take a random  $k$  between 1 and 5 and train the model with it. We evaluate the performance on inference with  $k = 3$  (the average value). In Fig. 7 we compare the performance of the best model trained with random number of iterations  $k$  with the best performing models trained with fixed  $k$ . As the plots show, the model trained with a random number of iterations performs on par with the best models with fixed  $k$ , but takes more time to train.

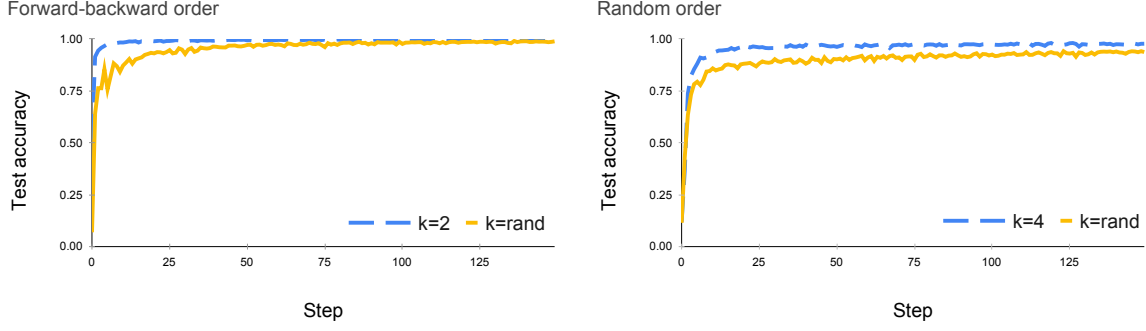


Figure 7: Learning curves for random number of variable update passes - for “forward-backward” and random order of operation updates.

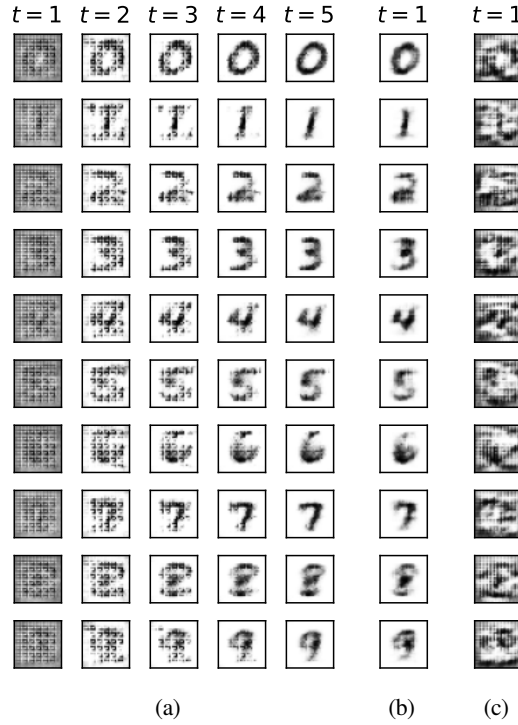


Figure 8: Digit prototypes generated by convolutional UNN. (a) best UNN ( $k=5, \alpha=.1$ ), (b) single iteration UNN ( $k=1, \alpha=.1$ ), (c): standard convnet ( $k=1, \alpha=0$ ). Extended version of Fig. 3.

### C. Additional visualizations

**MNIST digit prototypes.** Figure 8 shows the prototypes induced by an undirected convnet (a,b) and a standard feed-forward one (c) for all classes 0–9.

**Undirected self-attention weights.** In Fig. 9 we show an example of the weights of the undirected self-attention described in Section 3. The attention weights are the values of the variable  $S$  calculated in the forward and backward pass.

**Dependency tree packed representation** Figure 10 shows an example of how the trees are represented in the output of the model in Section 4.

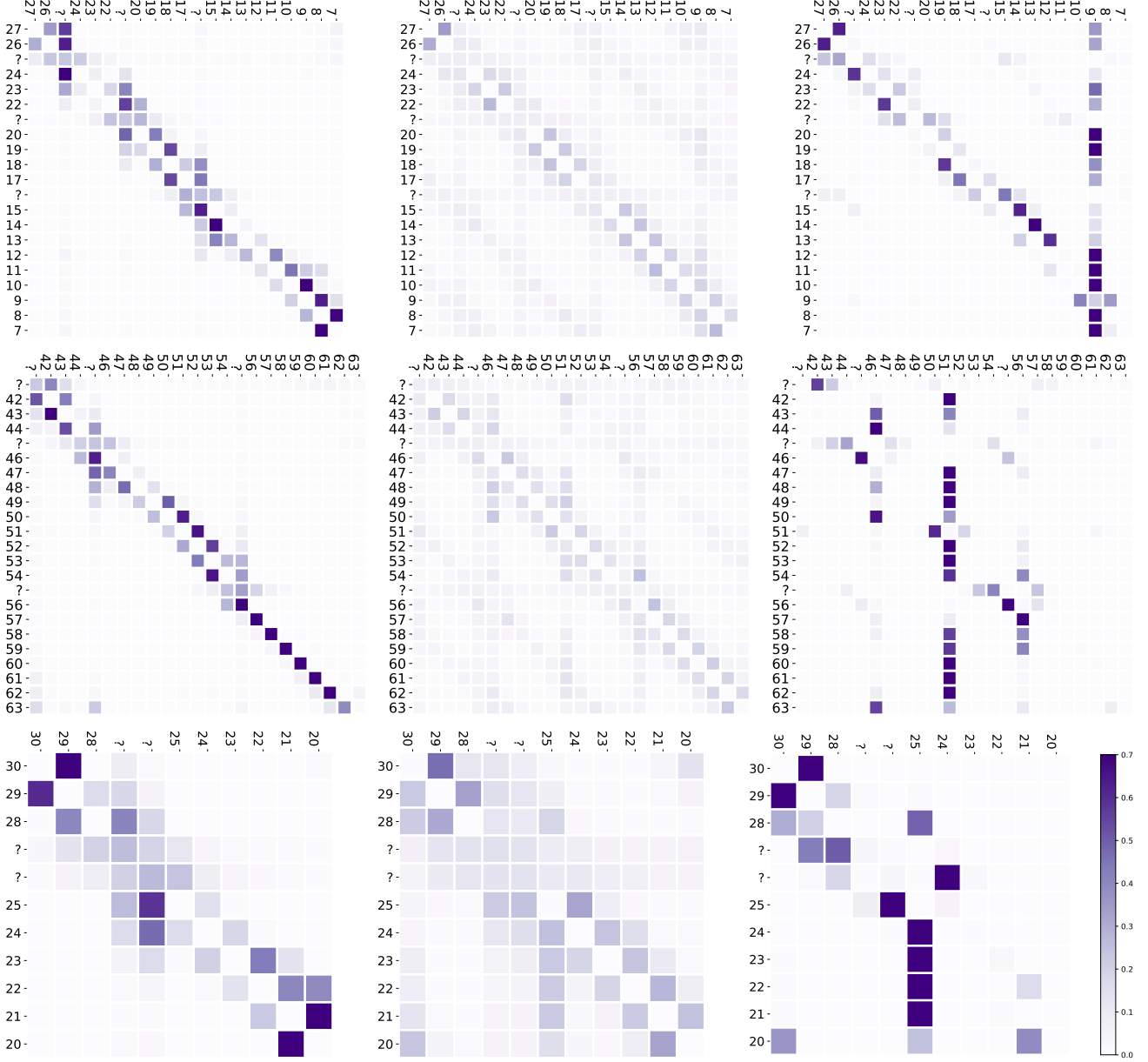


Figure 9: Example of the self-attention weights for models trained with  $k = 1$  (left) and  $k = 2$  after one iteration (middle) and two iterations (right). For  $k = 2$ , the model is more like an unrolled two-layer attention mechanism, with the first step identifying an off-diagonal pattern and the latter pooling information into an arbitrary token.

## D. Derivation of updates for convolutional UNN

The two-layer convolutional UNN is defined by the pairwise energies

$$\begin{aligned}
 E_{X H_1}(X, H_1) &= -\langle H_1, \mathcal{C}_1(X; W_1) \rangle, \\
 E_{H_1 H_2}(H_1, H_2) &= -\langle H_2, \mathcal{C}_2(H_1; W_2) \rangle, \\
 E_{H_2 Y}(H_2, y) &= -\langle y, V H_2 \rangle,
 \end{aligned} \tag{24}$$

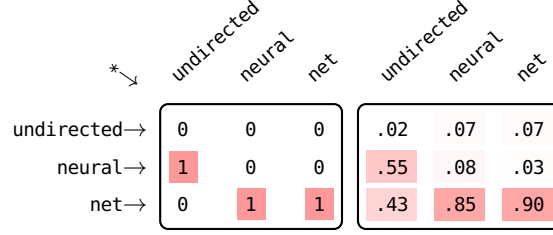


Figure 10: “Packed” matrix representation of a dependency tree (left) and dependency arc marginals (right). Each element corresponds to an arc  $h \rightarrow m$ , and the diagonal corresponds to the arcs from the root,  $* \rightarrow m$ . The marginals, computed via the matrix-tree theorem, are the structured counterpart of softmax, and correspond to arc probabilities.

and the unary energies

$$\begin{aligned}
E_X(X) &= \frac{1}{2} \|X\|_2^2, \\
E_{H_1}(H_1) &= -\langle H_1, b_1 \otimes 1_{d_1} \rangle + \Psi_{\tanh}(H_1), \\
E_{H_2}(H_2) &= -\langle H_2, b_2 \otimes 1_{d_2} \rangle + \Psi_{\tanh}(H_2), \\
E_Y(y) &= -\langle b, y \rangle - \mathcal{H}(y).
\end{aligned} \tag{25}$$

Above,  $\mathcal{C}_1$  and  $\mathcal{C}_2$  are linear cross-correlation (convolution) operators with stride two and filter weights  $W_1 \in \mathbb{R}^{32 \times 1 \times 6 \times 6}$  and  $W_2 \in \mathbb{R}^{64 \times 32 \times 4 \times 4}$ , and  $b_1 \in \mathbb{R}^{32}$  and  $b_2 \in \mathbb{R}^{64}$  are vectors of biases for each convolutional filter. The hidden activations have dimension  $H_1 \in \mathbb{R}^{32 \times (d_1)}$  and  $H_2 \in \mathbb{R}^{64 \times (d_2)}$ , where  $d_1$  and  $d_2$  are tuples that depend on the input image size; for MNIST,  $X \in \mathbb{R}^{1 \times 28 \times 28}$  leading to  $d_1 = 12 \times 12$  and  $d_2 = 5 \times 5$ .

To derive the energy updates, we use the fact that a real linear operator  $\mathcal{A}$  interacts with the Frobenius inner product as:

$$\langle P, \mathcal{A}(Q) \rangle = \langle Q, \mathcal{A}^\top(P) \rangle, \tag{26}$$

where  $\mathcal{A}^\top$  is the transpose, or adjoint, operator.<sup>3</sup> If  $\mathcal{C}$  is a convolution (*i.e.*, `torch.conv2d`) then  $\mathcal{C}^\top$  is a deconvolution (*i.e.*, `torch.conv_ttranspose2d`) with the same filters. We then have

$$\begin{aligned}
E_{X H_1}(X, H_1) &= -\langle H_1, \mathcal{C}_1(X; W_1) \rangle = -\langle X, \mathcal{C}_1^\top(H_1; W_1) \rangle, \\
E_{H_1 H_2}(H_1, H_2) &= -\langle H_2, \mathcal{C}_2(H_1; W_2) \rangle = -\langle H_1, \mathcal{C}_2^\top(H_2; W_2) \rangle.
\end{aligned} \tag{27}$$

Adding up all energies and ignoring the constant terms in each update, we get

$$\begin{aligned}
X_\star &= \operatorname{argmin}_X -\langle X, \mathcal{C}_1^\top(H_1; W_1) \rangle + \Psi_{\tanh}(X) \\
&= \tanh(\mathcal{C}_1^\top(H_1; W_1)), \\
(H_1)_\star &= \operatorname{argmin}_{H_1} -\langle H_1, \mathcal{C}_1(X; W_1) \rangle - \langle H_1, \mathcal{C}_2^\top(H_2; W_2) \rangle - \langle H_1, b_1 \otimes 1_{d_1 \times d_1} \rangle + \Psi_{\tanh}(H_1) \\
&= \tanh(\mathcal{C}_1(X; W_1) + \mathcal{C}_2^\top(H_2; W_2) + b_1 \otimes 1_{d_1 \times d_1}), \\
(H_2)_\star &= \operatorname{argmin}_{H_2} -\langle H_2, \mathcal{C}_2(H_1; W_2) \rangle - \langle H_2, \sigma_y(V)y \rangle - \langle H_2, b_2 \otimes 1_{d_2 \times d_2} \rangle + \Psi_{\tanh}(H_2) \\
&= \tanh(\mathcal{C}_2(H_1; W_2) + \sigma_y(V)y + b_2 \otimes 1_{d_2 \times d_2}), \\
y_\star &= -\langle y, V H_2 \rangle - \langle y, b \rangle - \mathcal{H}y \\
&= \operatorname{softmax}(V H_2 + b).
\end{aligned} \tag{28}$$

Note that in our case,  $H_2 \in \mathbb{R}^{64 \times 5 \times 5}$ ,  $V \in \mathbb{R}^{10 \times 64 \times 5 \times 5}$  and thus  $V H_2 \in \mathbb{R}^{10}$  is a tensor contraction (*e.g.*, `torch.tensordot(V, H_2, dims=3)`). The  $\sigma_y$  linear operator – opposite of  $\rho$  from Lemma 1 – rolls the axis of  $V$  corresponding to  $y$  to the *last* position, such that  $\sigma_y(V) \in \mathbb{R}^{64 \times 5 \times 5 \times 10}$ , the tensor analogue of a transposition (*e.g.*, `torch.permute(V, (1, 2, 3, 0))`).

<sup>3</sup>This generalizes the observation that  $p^\top A q = q^\top A^\top p$ .